

Mass spectra of bottom-charm baryons

Zhen-Yu Li^{1,*}, Guo-Liang Yu^{2,†}, Zhi-Gang Wang^{2,‡}, Jian-Zhong Gu³, and Hong-Tao Shen⁴

¹ School of Physics and Electronic Science,
Guizhou Education University, Guiyang 550018, China

² Department of Mathematics and Physics,
North China Electric Power University, Baoding 071003, China
³ China Institute of Atomic Energy, Beijing 102413, China
⁴ Guangxi Key Laboratory of Nuclear Physics and Technology,
Guangxi Normal University, Guilin 541006, China

(Dated: March 29, 2023)

In this paper, we investigate the mass spectra of bottom-charm baryons systematically, where the relativistic quark model and the infinitesimally shifted Gaussian basis function method are employed. Our calculation shows that the ρ -mode appears lower in energy than the other excited modes. According to this feature, the allowed quantum states are selected and a systematic study of the mass spectra for Ξ'_{bc} (Ξ_{bc}) and Ω'_{bc} (Ω_{bc}) families is performed. The root mean square radii and quark radial probability density distributions of these baryons are analyzed as well. Next, the Regge trajectories in the (J, M^2) plane are successfully constructed based on the mass spectra. At last, we present the structures of the mass spectra, and analyze the difficulty and opportunity in searching for the ground states of bottom-charm baryons in experiment.

Key words: Bottom-charm baryons, Mass spectra, Relativistic quark model.

PACS numbers: 13.25.Ft; 14.40.Lb

I. Introduction

Quantum chromodynamics (QCD) predicts the existence of baryons with two heavy quarks (b, c) and one light quark, known as the doubly heavy baryons (DHBs). DHBs can be divided into three groups: double-charm baryons (Ξ_{cc} and Ω_{cc}), double-bottom baryons (Ξ_{bb} and Ω_{bb}), and bottom-charm baryons (Ξ_{bc} and Ω_{bc}). The study of DHBS contributes to an in-depth understanding of the heavy quark symmetry, chiral dynamics, fundamental theory of the strong interaction, and models inspired by QCD.

*Electronic address: zhenyvli@163.com

†Electronic address: yuguoliang2011@163.com

‡Electronic address: zgwang@aliyun.com

The experimental research of DHBs was full of twists and turns. The Ξ_{cc}^+ baryon was first observed by the SELEX collaboration in 2002 [1]. But, other experiments have failed to confirm this so far. The experimental turning point for DHBS research occurred in 2017. Observations of Ξ_{cc}^{++} baryons were reported by the LHCb collaboration that year and have been confirmed several times since [2–4]. Now, the Ξ_{cc}^{++} baryon has become the first DHB collected in the new PDG data [5]. It opened the door to the experimental detection of DHBs, and people expected to find more DHBs experimentally. However, in the next experiments of searching for the Ξ_{bc}^0 [6], Ω_{bc}^0 [7] and Ξ_{bc}^+ [8] baryons, the LHCb collaboration observed no significant signals in the invariant mass range of $6.7 \sim 7.3$ GeV. So far, the DHB containing bottom quark has not yet been discovered experimentally.

The zero result of searching for the bottom-charm baryons has aroused great concern. Many theoretical efforts have been carried out to predict the production in the collider [9–16], the decay properties [17–29] and the accurate mass spectrum [30–63] of DHBs, so as to provide more powerful theoretical supports to the related experiments in the near future.

Recently, we have developed an approximate method [64, 65] to analyze the singly heavy baryon spectra systematically in which the relativistic quark model [66, 67] and the infinitesimally shifted Gaussian (ISG) basis function method [68] are employed. The result indicates that this method is reasonable and effective in the singly heavy baryon spectroscopy. Additionally, it is worth pointing out that these calculations are based on a uniform set of parameters [64, 65]. Then, we extended this method to study the mass spectra of the double charm baryons (Ξ_{cc} and Ω_{cc}) [69] and the double bottom baryons (Ξ_{bb} and Ω_{bb}) [70]. In the following sections, the systematic calculation of the bottom-charm baryon spectra by this method will be performed.

This paper is organized as follows. In Sect.II, the calculation method used in this work is briefly introduced. In Sect.III, we present the calculation results of the bottom-charm baryons, including the root mean square (r.m.s.) radii, mass spectra, quark radial probability density distributions, Regge trajectories and spectral structure, and give discussions about the results. Sect.IV is reserved for our conclusions.

II. Phenomenological methods adopted in this work

In our calculations, the relativistic quark model is employed to investigate the full mass spectra. In order to improve the computational accuracy and efficiency, the ISG method is also adopted in our studies. The relevant technical details can be found in references [64–68]. Next, we mainly introduce the selection of Jacobi coordinates and the structure of functions for bottom-charm baryons. The DHB is regarded as a three-quark system and the related calculation is performed in the Jacobi coordinates

as shown in Fig.1. There are three channels of Jacobi coordinates, which are defined as

$$\rho_i = \mathbf{r}_j - \mathbf{r}_k, \quad (1)$$

$$\lambda_i = \mathbf{r}_i - \frac{m_j \mathbf{r}_j + m_k \mathbf{r}_k}{m_j + m_k}, \quad (2)$$

where $i, j, k = 1, 2, 3$ (or replace their positions in turn). \mathbf{r}_i and m_i stand for the position vector and the mass of the i th quark, respectively.

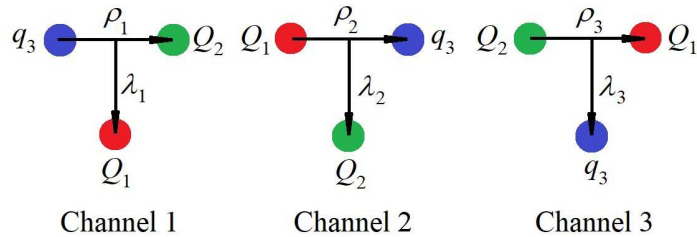


FIG. 1: (Color online) Jacobi coordinates for the three-quark system. The 3rd particle is specified as the light quark in the case of DHBs.

In our previous study of the double-bottom or -charm baryons [69, 70], the calculation result shows that the two heavy quarks in a baryon are bonded tightly. So, these two heavy quarks can be described as a subsystem, and channel 3 is a good picture to describe this situation. Similarly, the calculations in this work are also based on channel 3, where the 3rd quark is specified as the light quark and the flavor wave function in the subspace of the two heavy quarks (bc) can be expressed as,

$$\begin{aligned} \Xi_{bc} &= \frac{1}{\sqrt{2}}(bc - cb)q, \\ \Xi'_{bc} &= \frac{1}{\sqrt{2}}(bc + cb)q. \end{aligned} \quad (3)$$

Here q denotes up quark (u) or down quark (d). For Ω_{bc} and Ω'_{bc} , q is replaced by strange quark.

In channel 3, $\mathbf{l}_{\rho 3}$ (denoted in short as \mathbf{l}_ρ) stands for the orbital angular momentum between the two heavy quarks, and $\mathbf{l}_{\lambda 3}$ (denoted in short as \mathbf{l}_λ) represents the one between the bottom-charm quark pair and the light quark. For a quantum state in this work, the spatial wave function is combined with the spin function as follow,

$$|l_\rho \ l_\lambda \ L \ s \ j \ J \ M_J\rangle = \{[(|l_\rho \ m_\rho\rangle |l_\lambda \ m_\lambda\rangle)_L \times (|s_1 \ m_{s_1}\rangle |s_2 \ m_{s_2}\rangle)_s]_j \times |s_3 \ m_{s_3}\rangle\}_{JM_J}. \quad (4)$$

l_ρ , l_λ , L , s , j , J and M_J are the quantum numbers. The total spin s of (bc) and their orbital quantum number l_ρ should meet the following condition: $(-1)^{s+l_\rho} = 1$ for $\Xi_{bc}(\Omega_{bc})$ and $(-1)^{s+l_\rho} = -1$ for $\Xi'_{bc}(\Omega'_{bc})$, which guarantees the antisymmetry of the total wave function.

III. Numerical results and discussion

3.1 ρ -mode

As usual, $nL(J^P)$ is used to describe a baryon state. For the excited states ($L \neq 0$), there exist several $|l_\rho l_\lambda L s j J M_J\rangle$ states under the condition of $\mathbf{L} = \mathbf{l}_\rho + \mathbf{l}_\lambda$. They may be divided into the following three modes: (1) The ρ -mode with $l_\rho \neq 0$ and $l_\lambda = 0$; (2) The λ -mode with $l_\rho = 0$ and $l_\lambda \neq 0$; (3) The λ - ρ mixing mode with $l_\rho \neq 0$ and $l_\lambda \neq 0$. As an approximation, we take no account of the mixing of these modes, and note that the most likely mode to be observed experimentally should be that with lower energy. With this in mind, we need to analyze which mode has the lowest energy in our calculations.

Considering the excitation energies of the $1D(\frac{3}{2}^+, \frac{5}{2}^+)_{j=2}$ states for $\Xi'_{QQ'}$ and $\Xi_{QQ'}$ as functions of m_2 , we investigate the trend of these three modes in the heavy quark limit. Meanwhile, the dependence of excitation energies on m_2 of the ρ -mode is compared with that of the other two modes. Being $m_c = 1.628$ GeV and $m_b = 4.977$ GeV in the actual calculations below, we set $m_1 = (m_c/m_b)m_2$ here to keep them in proportion. From Fig.2, one can see that the excitation energies of the ρ -mode are significantly lower than those of the other two modes when m_2 increases from 2.0 GeV to 5.0 GeV. This suggests that the ρ -mode appears lower in energy than the other two modes in the heavy quark limit for bottom-charm baryons. Therefore, we only study the ρ -mode in this work. Additionally, the excitation energy differences between the $1D(\frac{3}{2}^+, \frac{5}{2}^+)_{j=2}$ states in the ρ -mode get closer to each other with increasing m_2 as shown in Fig.2, which is consistent with the heavy quark spin symmetry [71].

3.2 Mass spectra, r.m.s. radii and quark radial probability density distributions

In the ρ -mode, the complete mass spectra of the Ξ'_{bc} , Ξ_{bc} , Ω'_{bc} and Ω_{bc} baryons with quantum numbers up to $n = 4$ and $L = 4$ are calculated. The corresponding r.m.s. radii and part of the quark radial probability density distributions are computed as well. The detailed results are presented in Tables I-IV and Figs.3-6.

From Tables I-IV, one can find some general features as follows: (1) For the spin-doublet states with the same j , the $J = j + \frac{1}{2}$ state is higher in energy than the $J = j - \frac{1}{2}$ state. (2) For the same L , the mass splitting among different states becomes larger and larger with the increase of j . For example, Table I shows the mass differences (splittings) of the $1D$ doublets with $j = 1, 2, 3$ are 21 MeV, 35 MeV and 50 MeV, respectively. So, the mass splitting of the bottom-charm baryons shows the same feature as those of the double-charm and -bottom baryons [69, 70]. Moreover, by comparing the mass splittings of these three groups of the DHBs, one can find that this mass splitting is inversely

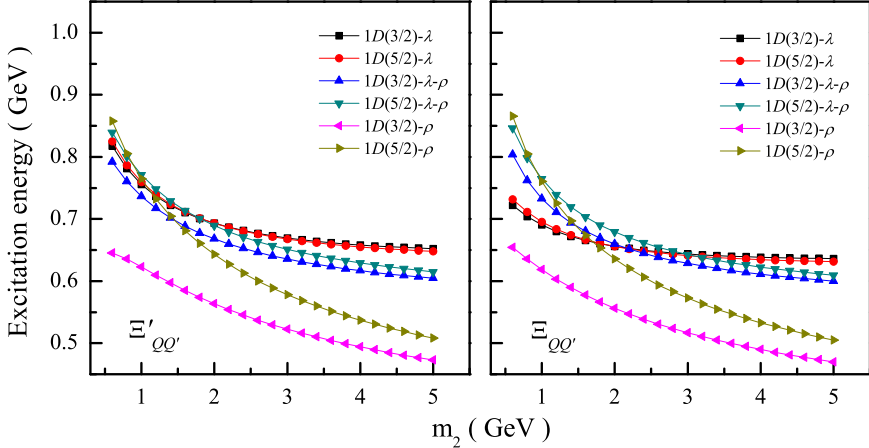


FIG. 2: (Color online) The dependence of excitation energies on m_2 for different modes of $\Xi'_{QQ'}$ and $\Xi_{QQ'}$, where $m_1 = (m_c/m_b)m_2$ and $m_3 = m_{u(d)}$. The excitation energies are measured from the ground states $1S(\frac{1}{2})_{j=1}^+$ of $\Xi'_{QQ'}$ and $1S(\frac{1}{2})_{j=0}^+$ of $\Xi_{QQ'}$, respectively.

proportional to the total mass of the heavy quark pair. (3) The mass difference between two adjacent radial excited states gradually decreases with increasing n . This is a general property for singly and doubly heavy baryons in our calculations.

The radial probability densities $\omega(r_\rho)$ and $\omega(r_\lambda)$ in a three-quark system can be defined below,

$$\begin{aligned}\omega(r_\rho) &= \int |\Psi(\mathbf{r}_\rho, \mathbf{r}_\lambda)|^2 d\mathbf{r}_\lambda d\Omega_\rho, \\ \omega(r_\lambda) &= \int |\Psi(\mathbf{r}_\rho, \mathbf{r}_\lambda)|^2 d\mathbf{r}_\rho d\Omega_\lambda,\end{aligned}\quad (5)$$

where Ω_ρ and Ω_λ stand for the solid angles spanned by vectors \mathbf{r}_ρ and \mathbf{r}_λ , respectively. Through the analyses of the quark radial probability density distributions in Figs.3-6 and the r.m.s. radii in Tables I-IV, one can find some interesting properties.

(1) The $\langle r_\rho^2 \rangle^{1/2}$ value of a ground state is smaller than the corresponding $\langle r_\lambda^2 \rangle^{1/2}$ value. This means that the two heavy quarks are bonded tightly. By using the results of our previous papers [69, 70] and examining the r.m.s. radii of these three groups of DHBs, one can find the $\langle r_\rho^2 \rangle^{1/2}$ value is also inversely proportional to the total mass of the heavy quark pair.

(2) Tables I-IV show that when n is fixed, $\langle r_\rho^2 \rangle^{1/2}$ values become larger with increasing L . Figs.3-6 also show a consistent change trend for the distribution of the $r_\rho^2 \omega(r_\rho)$ (solid lines), especially in the case of $n=1$ or 3, where the peak of $r_\rho^2 \omega(r_\rho)$ is significantly shifted outward with increasing L .

(3) The curves in Fig.3 are very similar to those in Fig.4 and the values of the r.m.s. radii in Tables I and II are also very close to each other for the same $nL(J^P)_j$ state. This suggests that the flavor

symmetry has only a little effect on the shapes of the bottom-charm baryons and their mass values.

(4) Although the difference of the curves in Fig.3 (or 4) and Fig.5 (or 6) is very small, for the same quantum state, the apparent differences can be seen in the $\langle r_\lambda^2 \rangle^{1/2}$ values and the mass values for Ξ_{bc}' and Ω_{bc} as shown in Table I and III. This reflects the different contributions to these physical quantities from up (down) quark and strange quark in bottom-charm baryons.

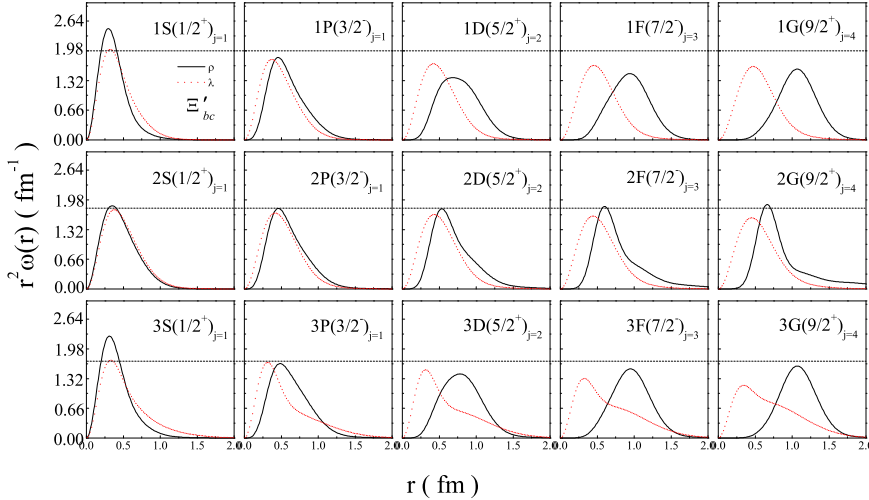


FIG. 3: (Color online) Quark radial probability density distributions for some nL states in the Ξ'_{bc} family. The solid line denotes the probability density with r_ρ , and the dash line the one with r_λ .

3.3 Regge trajectories

As an effective phenomenological approach, the Regge trajectory [72–75] can help ones to predict the evolution trend of hadron mass spectra. In turn, it could deepen our understanding of the hadron structure by testing the universality of the Regge theory.

In this paper, the following definition for the (J, M^2) Regge trajectories is used.

$$M^2 = \alpha J + \beta, \quad (6)$$

where α and β are the slope and intercept. In Fig.7, the Regge trajectories are plotted in the (J, M^2) plane based on the calculated mass spectra. The fitted slopes and intercepts of the Regge trajectories are given in Table V.

As shown in Fig.7, the group of $\Xi'_{bc}(NP)$ with the natural parity of $(-1)^{J-1/2}$ is composed of $S(\frac{1}{2}^+)_j=1$, $P(\frac{3}{2}^-)_j=1$, $D(\frac{5}{2}^+)_j=2$, $F(\frac{7}{2}^-)_j=3$ and $G(\frac{9}{2}^+)_j=4$ states. The group of $\Xi'_{bc}(UP)$ with the

TABLE I: The root mean square radii (fm) and mass spectra (MeV) of the Ξ_{bc}' family.

l_ρ	l_λ	L	s	j	$nL(J^P)$	$\langle r_\rho^2 \rangle^{1/2}$	$\langle r_\lambda^2 \rangle^{1/2}$	mass	l_ρ	l_λ	L	s	j	$nL(J^P)$	$\langle r_\rho^2 \rangle^{1/2}$	$\langle r_\lambda^2 \rangle^{1/2}$	mass
0 0 0 1 1					$1S(\frac{1}{2}^+)$	0.379	0.469	6952	2 0 2 1 3					$1D(\frac{7}{2}^+)$	0.749	0.566	7470
					$2S(\frac{1}{2}^+)$	0.691	0.555	7346						$2D(\frac{7}{2}^+)$	0.952	0.602	7747
					$3S(\frac{1}{2}^+)$	0.429	0.831	7455						$3D(\frac{7}{2}^+)$	0.792	0.925	7922
					$4S(\frac{1}{2}^+)$	1.072	0.610	7673						$4D(\frac{7}{2}^+)$	1.521	0.685	8011
0 0 0 1 1					$1S(\frac{3}{2}^+)$	0.382	0.488	6980	3 0 3 0 3					$1F(\frac{5}{2}^-)$	0.888	0.549	7598
					$2S(\frac{3}{2}^+)$	0.694	0.574	7368						$2F(\frac{5}{2}^-)$	1.022	0.570	7862
					$3S(\frac{3}{2}^+)$	0.432	0.841	7470						$3F(\frac{5}{2}^-)$	0.941	0.922	8051
					$4S(\frac{3}{2}^+)$	1.080	0.628	7692						$4F(\frac{5}{2}^-)$	1.678	0.663	8109
1 0 1 0 1					$1P(\frac{1}{2}^-)$	0.566	0.504	7223	3 0 3 0 3					$1F(\frac{7}{2}^-)$	0.899	0.592	7642
					$2P(\frac{1}{2}^-)$	0.838	0.561	7538						$2F(\frac{7}{2}^-)$	1.035	0.611	7907
					$3P(\frac{1}{2}^-)$	0.609	0.872	7705						$3F(\frac{7}{2}^-)$	0.946	0.952	8082
					$4P(\frac{1}{2}^-)$	1.321	0.637	7840						$4F(\frac{7}{2}^-)$	1.668	0.700	8142
1 0 1 0 1					$1P(\frac{3}{2}^-)$	0.571	0.523	7247	4 0 4 1 3					$1G(\frac{5}{2}^+)$	1.029	0.572	7759
					$2P(\frac{3}{2}^-)$	0.841	0.579	7559						$2G(\frac{5}{2}^+)$	1.097	0.579	8024
					$3P(\frac{3}{2}^-)$	0.610	0.884	7719						$3G(\frac{5}{2}^+)$	1.078	0.946	8199
					$4P(\frac{3}{2}^-)$	1.326	0.654	7856						$4G(\frac{5}{2}^+)$	1.806	0.675	8236
2 0 2 1 1					$1D(\frac{1}{2}^+)$	0.728	0.534	7431	4 0 4 1 3					$1G(\frac{7}{2}^+)$	1.039	0.614	7800
					$2D(\frac{1}{2}^+)$	0.940	0.572	7708						$2G(\frac{7}{2}^+)$	1.121	0.621	8067
					$3D(\frac{1}{2}^+)$	0.777	0.902	7896						$3G(\frac{7}{2}^+)$	1.085	0.975	8228
					$4D(\frac{1}{2}^+)$	1.522	0.660	7986						$4G(\frac{7}{2}^+)$	1.786	0.710	8267
2 0 2 1 1					$1D(\frac{3}{2}^+)$	0.733	0.552	7452	4 0 4 1 4					$1G(\frac{7}{2}^+)$	1.030	0.566	7751
					$2D(\frac{3}{2}^+)$	0.943	0.590	7728						$2G(\frac{7}{2}^+)$	1.097	0.572	8017
					$3D(\frac{3}{2}^+)$	0.778	0.915	7909						$3G(\frac{7}{2}^+)$	1.080	0.942	8193
					$4D(\frac{3}{2}^+)$	1.521	0.676	8001						$4G(\frac{7}{2}^+)$	1.806	0.668	8229
2 0 2 1 2					$1D(\frac{3}{2}^+)$	0.731	0.528	7425	4 0 4 1 4					$1G(\frac{9}{2}^+)$	1.043	0.620	7803
					$2D(\frac{3}{2}^+)$	0.941	0.566	7703						$2G(\frac{9}{2}^+)$	1.129	0.628	8073
					$3D(\frac{3}{2}^+)$	0.781	0.899	7892						$3G(\frac{9}{2}^+)$	1.088	0.980	8230
					$4D(\frac{3}{2}^+)$	1.522	0.654	7981						$4G(\frac{9}{2}^+)$	1.780	0.714	8270
2 0 2 1 2					$1D(\frac{5}{2}^+)$	0.740	0.559	7460	4 0 4 1 5					$1G(\frac{9}{2}^+)$	1.032	0.560	7743
					$2D(\frac{5}{2}^+)$	0.946	0.596	7736						$2G(\frac{9}{2}^+)$	1.100	0.566	8011
					$3D(\frac{5}{2}^+)$	0.784	0.920	7915						$3G(\frac{9}{2}^+)$	1.083	0.939	8186
					$4D(\frac{5}{2}^+)$	1.521	0.681	8006						$4G(\frac{9}{2}^+)$	1.804	0.662	8223
2 0 2 1 3					$1D(\frac{5}{2}^+)$	0.737	0.523	7420	4 0 4 1 5					$1G(\frac{11}{2}^+)$	1.047	0.626	7807
					$2D(\frac{5}{2}^+)$	0.943	0.561	7700						$2G(\frac{11}{2}^+)$	1.141	0.634	8079
					$3D(\frac{5}{2}^+)$	0.788	0.896	7890						$3G(\frac{11}{2}^+)$	1.093	0.984	8232
					$4D(\frac{5}{2}^+)$	1.524	0.648	7976						$4G(\frac{11}{2}^+)$	1.769	0.717	8273

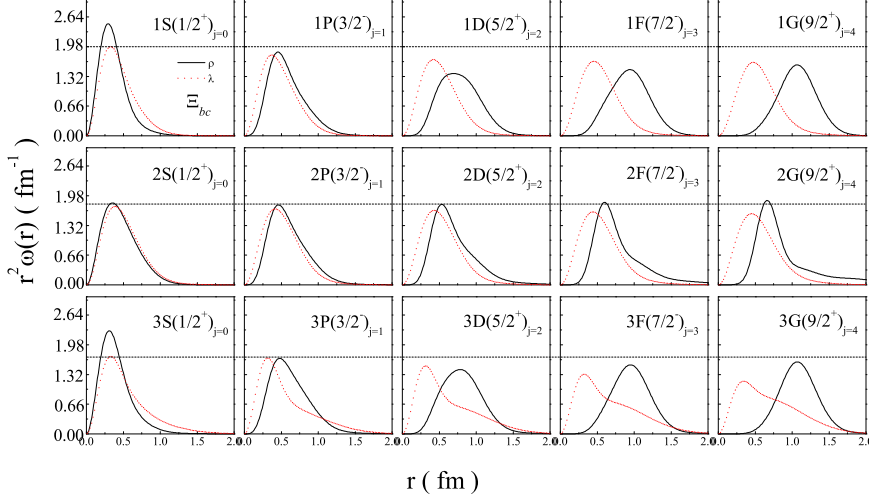


FIG. 4: (Color online) Same as Fig.3, but for the Ξ_{bc} family.

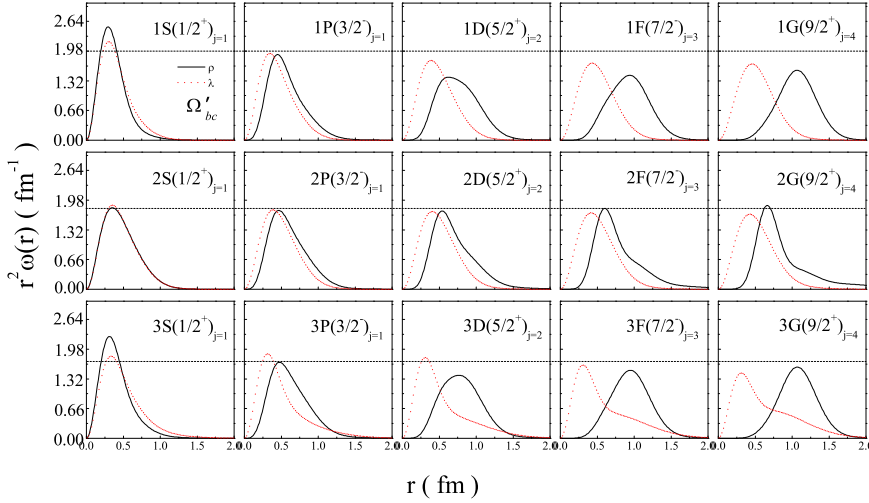


FIG. 5: (Color online) Same as Fig.3, but for the Ω'_{bc} family.

unnatural parity of $(-1)^{J+1/2}$ is composed of $P(\frac{1}{2}^-)_{j=1}$, $D(\frac{3}{2}^+)_{j=2}$, $F(\frac{5}{2}^-)_{j=3}$ and $G(\frac{7}{2}^+)_{j=4}$ states. For Ξ'_{bc} family, the remaining states in Table I can also be put into these lines, because their mass values are very near those states with the same $L(J^P)$. The situation is similar for Ξ_{bc} , Ω'_{bc} and Ω_{bc} families. From Fig.7, one can see that most of the data points fall on the trajectory lines.

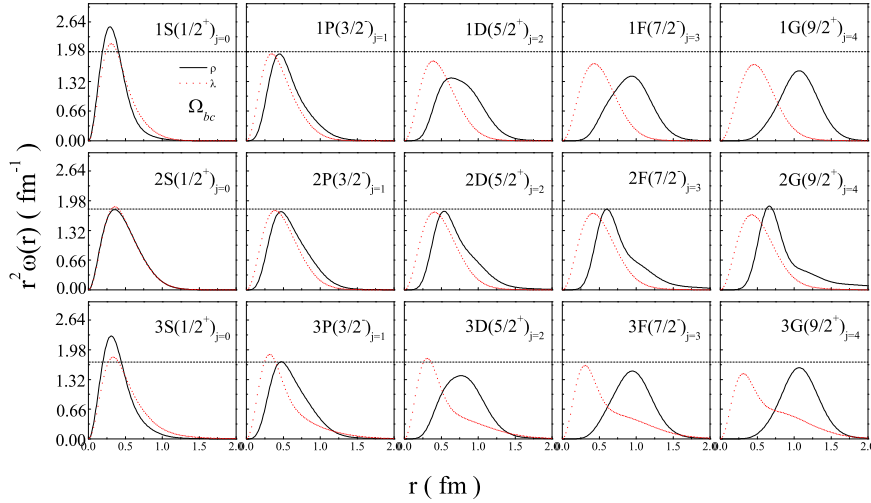


FIG. 6: (Color online) Same as Fig.3, but for the Ω_{bc} family.

By comparing the slope values in Table V with those of the double-charm and -bottom baryons [69, 70], we find a phenomenon: The slopes of the two lines with $n = 1$ and $n = 3$ are roughly the same. However, the slope of the line with $n = 2$ is different from those of the other two lines, and this difference becomes bigger with increasing the total mass of the heavy quark pair.

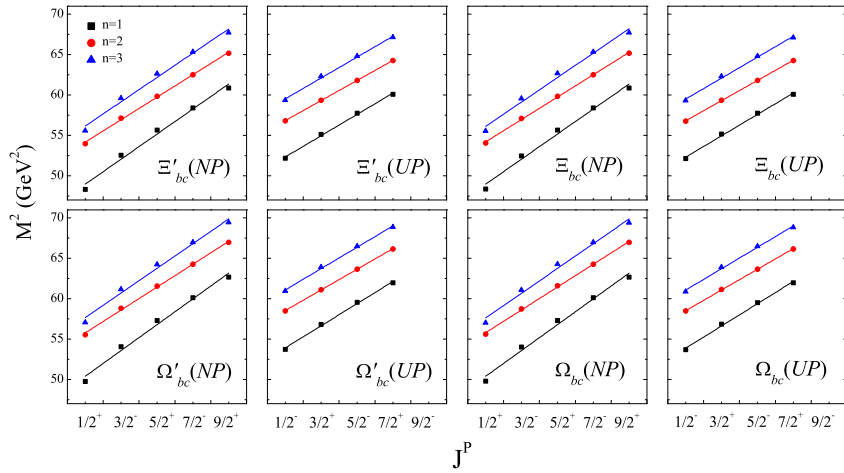


FIG. 7: (Color online) (J, M^2) Regge trajectories for the Ξ'_{bc} (Ξ_{bc}) and Ω'_{bc} (Ω_{bc}) families and M^2 is in GeV^2 . NP denotes the natural parity, and UP the unnatural parity.

3.4 Shell structure of the mass spectra

The spectral structures of the Ξ'_{bc} (Ξ_{bc}) and Ω'_{bc} (Ω_{bc}) baryons with $L \leq 2$ are presented in Figs.8 and 9, respectively. As shown in Fig.8, there are 3 members of the $1S$ -wave states for the Ξ'_{bc} and Ξ_{bc} families. The calculated masses are 6952 MeV for $1S(\frac{1}{2}^+)_{j=1}$ state, 6955 MeV for $1S(\frac{1}{2}^+)_{j=0}$ state, and 6980 MeV for $1S(\frac{3}{2}^+)_{j=1}$ state, respectively. One can see that the masses of these three states are relatively close, and the $1S(\frac{1}{2}^+)_{j=0}$ state of Ξ_{bc} lies between the $1S(\frac{1}{2}, \frac{3}{2})_{j=1}$ doublet states of Ξ'_{bc} . This suggests that there is a certain difficulty in the identification of the three $1S$ states in experiment. On the other hand, good news is that there lies a big gap (about 240 MeV) between the $1S$ and $1P$ sub-shells as shown in Fig.8. This implies the experimental measurement of the $1S$ states for the Ξ'_{bc} and Ξ_{bc} baryons could be done cleanly. The same is true for Ω'_{bc} and Ω_{bc} baryons as shown in Fig.9, where the calculated masses are 7053 MeV for $1S(\frac{1}{2}^+)_{j=1}$ state, 7055 MeV for $1S(\frac{1}{2}^+)_{j=0}$ state and 7079 MeV for $1S(\frac{3}{2}^+)_{j=1}$ state, respectively.

At last, the calculated masses of the $1S$ states in this work are compared with those given by some other theoretical methods as shown in Table VI. From Table VI, one can see that the masses by the other methods are mainly distributed in the range of 6800~7100 MeV for Ξ'_{bc} and Ξ_{bc} families, and 6900~7200 MeV for Ω'_{bc} and Ω_{bc} families. With the above masses, the average value for each $1S$ state is calculated. Table VI shows that our calculated masses are close to the average values in general.

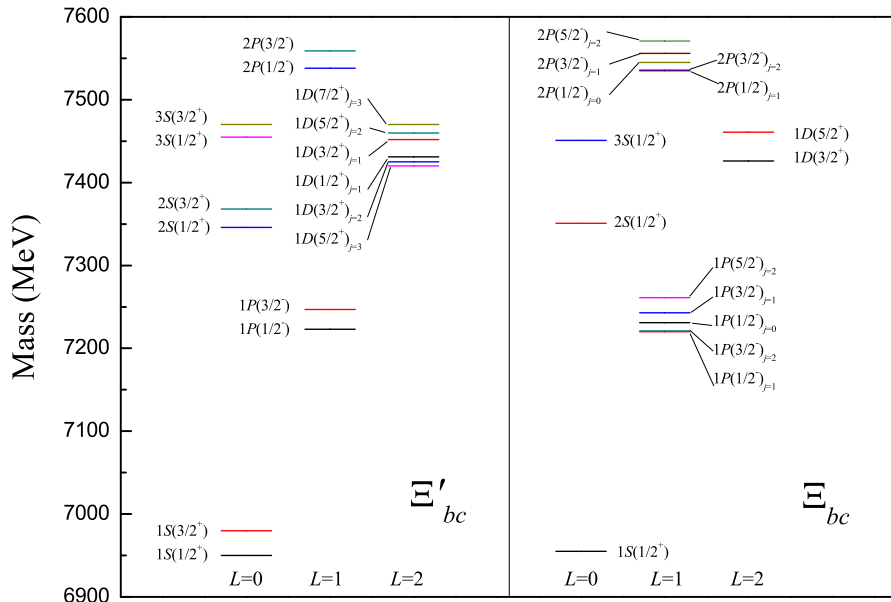


FIG. 8: (Color online)Shell structure of the Ξ'_{bc} (Ξ_{bc}) family.

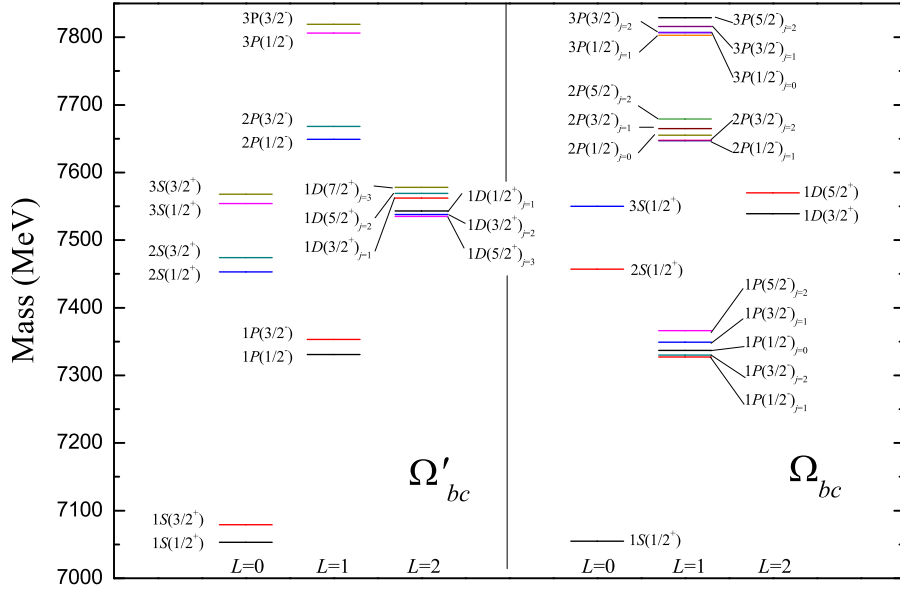


FIG. 9: (Color online) Same as Fig.8, but for the Ω'_bc (Ω_{bc}) family.

IV. Conclusions

In this work, by using the relativistic quark model and the ISG method, we investigate the bottom-charm baryon spectra systematically. In the ρ -mode, we obtain the mass spectra of the Ξ'_{bc} (Ξ_{bc}) and Ω'_{bc} (Ω_{bc}) families. The related r.m.s. radii and quark radial probability density distributions are investigated as well, from which we learn more about the structure of bottom-charm baryons.

Based on the obtained mass spectra, we construct successfully the Regge trajectories in the (J, M^2) plane. We find the slopes of the lines with $n = 2$ differ from those of the other lines with $n = 1$ and $n = 3$, and the difference changes regularly with increasing total mass of the two heavy quarks.

At last, the mass spectral structures of the Ξ'_{bc} (Ξ_{bc}) and Ω'_{bc} (Ω_{bc}) families are presented. We analyze the features of the mass spectral structures, and discuss the difficulty and opportunity of the experimental measurements for the $1S$ states in Ξ'_{bc} (Ξ_{bc}) and Ω'_{bc} (Ω_{bc}) families. We also compare our calculated masses of the $1S$ states with those given by some other theoretical methods. It turns out that our results are close to their average values in general.

Acknowledgements

This research is supported by the Central Government Guidance Funds for Local Scientific and Technological Development of China (No. Guike ZY22096024), the National Natural Science Foundation of China (Grant No. 11675265), the Continuous Basic Scientific Research Project (Grant No. WDJC-2019-13), and the Leading Innovation Project (Grant No. LC 192209000701).

- [1] M. Mattson et al. [SELEX Collaboration], Phys. Rev. Lett. 89 (2002), 112001.
- [2] R. Aaij et al. [LHCb Collaboration], Phys. Rev. Lett. 119 (2017), 112001, [arXiv:1707.01621].
- [3] R. Aaij et al. [LHCb Collaboration], Chin. Phys. C 44 (2020), 022001, [arXiv:1910.11316].
- [4] R. Aaij et al. [LHCb Collaboration], Phys. Rev. Lett. 121 (2018), 162002, [arXiv:1807.01919].
- [5] P. A. Zyla, et al. [Pa Data Group], Prog. Theor. Exp. Phys. 8 (2020), 083C01.
- [6] R. Aaij, et al. [LHCb Collaboration], JHEP 11 (2020), 095, [arXiv:2009.02481].
- [7] R. Aaij, et al. [LHCb Collaboration], Chin. Phys. C 45 (2021), 093002, [arXiv:2104.04759].
- [8] [LHCb Collaboration], [arXiv:2204.09541].
- [9] S. Koshkarev, Acta. Phys. Polon. B 48 (2017), 163, arXiv:1610.06125v4 [hep-ph].
- [10] H. Y. Bi, R. Y. Zhang, X. G. Wu, W. G. Ma, X. Z. Li, O. Samuel, Phys. Rev. D 95 (2017), 7, arXiv:1702.07181v3 [hep-ph].
- [11] A. Ali, A. Y. Parkhomenko, Q. Qin, W. Wang, Phys. Lett. B 782 (2018), 412-420, arXiv:1805.02535v2 [hep-ph].
- [12] A. Ali, Q. Qin, W. Wang, Phys. Lett. B 785 (2018), 605-609, arXiv:1806.09288[hep-ph].
- [13] A. V. Berezhnoy, A. K. Likhoded, A. V. Luchinsky, Phys. Rev. D 98 (2018) 11, 113004, arXiv:1809.10058[hep-ph].
- [14] J. J. Niu, L. Guo, H. H. Ma, X. G. Wu, X. C. Zheng, Phys. Rev. D 98 (2018) 9, 094021, arXiv:1810.03834[hep-ph].
- [15] J. M. Richard, A. Valcarce, J. Vijande, Bled Workshops Phys. 19 (2018) 24, arXiv:1811.02863[hep-ph].
- [16] X. Luo, H. B. Fu, H. J. Tian, arXiv:2208.07520[hep-ph].
- [17] R. H. Li, C. D. Lü, W. Wang, F. S. Yu, Z. T. Zou, Phys. Lett. B 767 (2017), 232-235, arXiv:1701.03284[hep-ph].
- [18] Z. X. Zhao, Eur. Phys. J. C 78 (2018) 9, 756, arXiv:1805.10878[hep-ph].
- [19] Q. A. Zhang, Eur. Phys. J. C 78 (2018) 12, 1024, arXiv:1811.02199[hep-ph].
- [20] Y. J. Shi, Y. Xing, Z. X. Zhao, Eur. Phys. J. C 80 (2020) 1, 56, arXiv:1903.03921[hep-ph].
- [21] H. Y. Cheng, F. R. Xu, Phys. Rev. D 99 (2019) 7, 073006, arXiv:1903.08148[hep-ph].
- [22] A. V. Luchinsky, A. K. Likhoded, Phys. Rev. D 102 (2020) 1, 014019, arXiv:2007.04010[hep-ph].
- [23] Z. P. Xing, Z. X. Zhao, Eur. Phys. J. C 81 (2021) 12, 1111, arXiv:2109.00216[hep-ph].
- [24] P. H. Zhang, L. Guo, X. C. Zheng, Q. W. Ke, Phys. Rev. D 105 (2022) 034016, arXiv:2202.01579[hep-ph].
- [25] X. H. Hu, Y. J. Shi, arXiv:2202.07540[hep-ph].

- [26] A. Kakadiya, C. Menapara, arXiv:2204.13438[hep-ph].
- [27] T. M. Aliev, M. Savci, S. Bilmis, Phys. Rev. D 106 (2022) 3, 034017, arXiv:2205.14012[hep-ph].
- [28] Z. Ghalenovi, M. M. Sorkhi, arXiv:2208.07625[hep-ph].
- [29] H. Liu, Z. P. Xing, C. Yang, arXiv:2210.10529[hep-ph].
- [30] X. Z. Weng, X. L. Chen, W. Z. Deng, Phys. Rev. D 97 (2018) 5, 054008, arXiv:1801.08644[hep-ph].
- [31] N. Mohajery, N. Salehi, H. Hassanabadi, Adv. High Energy Phys. 2018 (2018) 1326438, arXiv:1807.06800[hep-ph].
- [32] Z. G. Wang, Eur. Phys. J. C 78 (2018) 10, 826, arXiv:1808.09820[hep-ph].
- [33] Q. X. Yu, X. H. Guo, Nucl.Phys.B 947 (2019) 114727, arXiv:1810.00437[hep-ph].
- [34] X. C. Zheng, C. H. Chang, T. F. Feng, Sci. China Phys. Mech. Astron. 63 (2020) 8, 281011, arXiv:1810.09393[hep-ph].
- [35] Q. Li, C. H. Chang, S. X. Qin, G. L. Wang, Chin. Phys.C 44 (2020) 1, 013102, arXiv:1903.02282[hep-ph].
- [36] T. M. Aliev, S. Bilmis, Nucl. Phys. A 984 (2019) 99-111, arXiv:1904.11279[hep-ph].
- [37] P. Mohanta, S. Basak, Phys. Rev. D 101 (2020) 9, 094503, arXiv:1911.03741[hep-ph].
- [38] W. X. Zhang, H. Xu, D. J. Jia, Phys. Rev. D 104 (2021) 11, 114011, arXiv:2109.07040[hep-ph].
- [39] H. Z. Tong, H. S. Li, Commun. Theor. Phys. 74 (2022) 8, 085201, arXiv:2110.01380[hep-ph].
- [40] J. T. Castellà, EPJ Web Conf. 258 (2022) 04003, arXiv:2111.09783[hep-ph].
- [41] Z. G. Wang, Q. Xin, Int. J. Mod. Phys. A 37 (2022) 2250074, arXiv:2202.03828[hep-ph].
- [42] T. Aliyev, S. Bilmış, Turk. J. Phys. 46 (2022) 1, 1-26, arXiv:2203.02965[hep-ph].
- [43] Y. X. Song, D. J. Jia, W. X. Zhang, A. Hosaka, arXiv:2204.00363[hep-ph].
- [44] Z. Ghalenovi, C. P. Shen, M. M. Sorkhi, Phys. Lett. B 834 (2022) 137405, arXiv:2204.02938[hep-ph].
- [45] J. Oudichhya, K. Gandhi, A. K. Rai, Phys. Scripta 97 (2022) 5, 054001, arXiv:2204.10045[hep-ph].
- [46] A. Kakadiya, C. Menapara, A. K. Rai, arXiv:2204.13438[hep-ph].
- [47] V. V. Kiselev, A. K. Likhoded, O. N. Pakhomova, V. A. Saleev, Int. J. Mod. Phys. D 12 (2003) 1415-1430, arXiv:0206140[hep-ph].
- [48] D. H. He, K. Qian, Y. B. Ding, X. Q. Li, P. N. Shen, Springer Proc. Phys. 99 (2005) 381-390, arXiv:0403301[hep-ph].
- [49] E. Bagan, H. G. Dosch, P. Gosdzinsky, S. Narison, J. M. Richard, Z. Phys. C 64 (1994) 57-72, arXiv:9403208[hep-ph].
- [50] D. Ebert, R. N. Faustov, V. O. Galkin, A. P. Martynenko, V. A. Saleev, Z. Phys. C 76 (1997) 111-115, arXiv:9607314[hep-ph].
- [51] J. R. Zhang, M. Q. Huang, Chin. Phys. C 33 (2009) 1385-1388, arXiv:0904.3391[hep-ph].
- [52] Z. G. Wang, Eur. Phys. J. A 45 (2010) 267-274, arXiv:1001.4693[hep-ph].
- [53] Z. G. Wang, Eur. Phys. J. C 68 (2010) 459-472, arXiv:1002.2471[hep-ph].
- [54] Z. G. Wang, Eur. Phys. J. A 47 (2011) 81, arXiv:1003.2838[hep-ph].
- [55] B. Eakins, W. Roberts, Int. J. Mod. Phys. A 27 (2012) 1250039, arXiv:1201.4885[hep-ph].
- [56] Z. G. Wang, Eur. Phys. J. C 72 (2012) 2099, arXiv:1205.0605[hep-ph].
- [57] T. M. Aliev, K. Azizi, M. Savci, Nucl. Phys. A 895 (2012) 59-70, arXiv:1205.2873[hep-ph].
- [58] T. M. Aliev, K. Azizi, M. Savci, Eur. J. Phys. G 40 (2013) 065003, arXiv:1208.1976[hep-ph].
- [59] Z. Ghalenovi, A. A. Rajabi, S. X. Qin, D. H. Rischke, Mod. Phys. Lett. A 29 (2014) 1450106,

- arXiv:1403.4582[hep-ph].
- [60] M. Karliner, J. L. Rosner, Phys. Rev. D 90 (2014) 9, 094007, arXiv:1408.5877[hep-ph].
- [61] Z. Shah, K. Thakkar, A. K. Rai, Eur. Phys. J. C 76 (2016) 10, 530, arXiv:1609.03030[hep-ph].
- [62] H. Garcilazo, A. Valcarce, J. Vijande, Phys. Rev. D 94 (2016) 7, 074003, arXiv:1609.06886[hep-ph].
- [63] Z. Shah, A. K. Rai, Eur. Phys. J. C 77 (2017) 2, 129, arXiv:1702.02726[hep-ph].
- [64] G. L. Yu, Z. Y. Li, Z. G. Wang, J. Lu, M. Yan, arXiv:2206.08128[hep-ph].
- [65] Z. Y. Li, G. L. Yu, Z. G. Wang, J. Z. Gu, J. Lu, arXiv:2207.04167[hep-ph].
- [66] S. Godfrey and N. Isgur, Phys. Rev. D 32 (1985), 189.
- [67] S. Capstick and N. Isgur, Phys. Rev. D 34, 2809 (1986).
- [68] E. Hiyama, Y. Kino and M. Kamimura, Prog. Part. Nucl. Phys. 51 (2003), 223.
- [69] G. L. Yu, Z. Y. Li, Z. G. Wang, J. Lu, M. Yan, arXiv:2211.00510 [hep-ph]
- [70] Z. Y. Li, G. L. Yu, Z. G. Wang, J. Z. Gu, arXiv:2210.13085 [hep-ph]
- [71] H. X. Chen, W. Chen, X. Liu et al., Rept. Prog. Phys. 80 (2017) 7, 076201 , arXiv:1609.08928[hep-ph].
- [72] T. Regge, Nuovo Cim. 14 (1959), 951.
- [73] T. Regge, Nuovo Cim. 18 (1960), 947-956.
- [74] G. F. Chew and S. C. Frautschi, Phys. Rev. Lett. 7 (1961), 394-397.
- [75] G. F. Chew and S. C. Frautschi, Phys. Rev. Lett. 8 (1962), 41-44.

TABLE II: The root mean square radii (fm) and mass spectra (MeV) of the Ξ_{bc} family.

l_ρ	l_λ	L	s	j	$nL(J^P)$	$\langle r_\rho^2 \rangle^{1/2}$	$\langle r_\lambda^2 \rangle^{1/2}$	mass	l_ρ	l_λ	L	s	j	$nL(J^P)$	$\langle r_\rho^2 \rangle^{1/2}$	$\langle r_\lambda^2 \rangle^{1/2}$	mass
0 0 0 0 0					$1S(\frac{1}{2}^+)$	0.370	0.479	6955	3 0 3 1 2					$1F(\frac{3}{2}^-)$	0.885	0.555	7605
					$2S(\frac{1}{2}^+)$	0.683	0.569	7351						$2F(\frac{3}{2}^-)$	1.021	0.575	7868
					$3S(\frac{1}{2}^+)$	0.422	0.834	7451						$3F(\frac{3}{2}^-)$	0.937	0.926	8056
					$4S(\frac{1}{2}^+)$	1.060	0.621	7677						$4F(\frac{3}{2}^-)$	1.679	0.670	8115
1 0 1 1 0					$1P(\frac{1}{2}^-)$	0.559	0.514	7231	3 0 3 1 2					$1F(\frac{5}{2}^-)$	0.893	0.585	7637
					$2P(\frac{1}{2}^-)$	0.835	0.572	7545						$2F(\frac{5}{2}^-)$	1.030	0.605	7900
					$3P(\frac{1}{2}^-)$	0.599	0.878	7707						$3F(\frac{5}{2}^-)$	0.940	0.947	8078
					$4P(\frac{1}{2}^-)$	1.315	0.648	7847						$4F(\frac{5}{2}^-)$	1.672	0.696	8138
1 0 1 1 1					$1P(\frac{1}{2}^-)$	0.562	0.503	7220	3 0 3 1 3					$1F(\frac{5}{2}^-)$	0.886	0.549	7598
					$2P(\frac{1}{2}^-)$	0.836	0.561	7535						$2F(\frac{5}{2}^-)$	1.021	0.570	7862
					$3P(\frac{1}{2}^-)$	0.604	0.871	7702						$3F(\frac{5}{2}^-)$	0.940	0.922	8051
					$4P(\frac{1}{2}^-)$	1.317	0.637	7838						$4F(\frac{5}{2}^-)$	1.679	0.664	8109
1 0 1 1 1					$1P(\frac{3}{2}^-)$	0.566	0.522	7243	3 0 3 1 3					$1F(\frac{7}{2}^-)$	0.898	0.591	7642
					$2P(\frac{3}{2}^-)$	0.839	0.578	7556						$2F(\frac{7}{2}^-)$	1.034	0.611	7907
					$3P(\frac{3}{2}^-)$	0.605	0.883	7716						$3F(\frac{7}{2}^-)$	0.944	0.951	8082
					$4P(\frac{3}{2}^-)$	1.322	0.654	7855						$4F(\frac{7}{2}^-)$	1.668	0.700	8142
1 0 1 1 2					$1P(\frac{3}{2}^-)$	0.572	0.499	7221	3 0 3 1 4					$1F(\frac{7}{2}^-)$	0.890	0.543	7591
					$2P(\frac{3}{2}^-)$	0.841	0.556	7536						$2F(\frac{7}{2}^-)$	1.023	0.564	7857
					$3P(\frac{3}{2}^-)$	0.616	0.869	7706						$3F(\frac{7}{2}^-)$	0.944	0.919	8047
					$4P(\frac{3}{2}^-)$	1.327	0.632	7837						$4F(\frac{7}{2}^-)$	1.678	0.657	8103
1 0 1 1 2					$1P(\frac{5}{2}^-)$	0.580	0.530	7261	3 0 3 1 4					$1F(\frac{9}{2}^-)$	0.905	0.598	7648
					$2P(\frac{5}{2}^-)$	0.846	0.585	7571						$2F(\frac{9}{2}^-)$	1.041	0.617	7914
					$3P(\frac{5}{2}^-)$	0.618	0.890	7730						$3F(\frac{9}{2}^-)$	0.951	0.957	8086
					$4P(\frac{5}{2}^-)$	1.334	0.660	7865						$4F(\frac{9}{2}^-)$	1.663	0.704	8145
2 0 2 0 2					$1D(\frac{3}{2}^+)$	0.733	0.529	7426	4 0 4 0 4					$1G(\frac{7}{2}^+)$	1.030	0.566	7751
					$2D(\frac{3}{2}^+)$	0.942	0.567	7704						$2G(\frac{7}{2}^+)$	1.099	0.573	8017
					$3D(\frac{3}{2}^+)$	0.783	0.899	7893						$3G(\frac{7}{2}^+)$	1.081	0.942	8192
					$4D(\frac{3}{2}^+)$	1.523	0.654	7981						$4G(\frac{7}{2}^+)$	1.805	0.668	8229
2 0 2 0 2					$1D(\frac{5}{2}^+)$	0.742	0.559	7461	4 0 4 0 4					$1G(\frac{9}{2}^+)$	1.043	0.620	7803
					$2D(\frac{5}{2}^+)$	0.948	0.596	7737						$2G(\frac{9}{2}^+)$	1.131	0.628	8073
					$3D(\frac{5}{2}^+)$	0.786	0.920	7916						$3G(\frac{9}{2}^+)$	1.089	0.980	8230
					$4D(\frac{5}{2}^+)$	1.521	0.681	8006						$4G(\frac{9}{2}^+)$	1.778	0.714	8270

TABLE III: The root mean square radii (fm) and mass spectra (MeV) of the Ω_{bc}' family.

l_ρ	l_λ	L	s	j	$nL(J^P)$	$\langle r_\rho^2 \rangle^{1/2}$	$\langle r_\lambda^2 \rangle^{1/2}$	mass	l_ρ	l_λ	L	s	j	$nL(J^P)$	$\langle r_\rho^2 \rangle^{1/2}$	$\langle r_\lambda^2 \rangle^{1/2}$	mass
0 0 0 1 1					$1S(\frac{1}{2}^+)$	0.371	0.429	7053	2 0 2 1 3					$1D(\frac{7}{2}^+)$	0.738	0.522	7578
					$2S(\frac{1}{2}^+)$	0.675	0.526	7453						$2D(\frac{7}{2}^+)$	0.942	0.558	7856
					$3S(\frac{1}{2}^+)$	0.438	0.771	7554						$3D(\frac{7}{2}^+)$	0.787	0.872	8022
					$4S(\frac{1}{2}^+)$	1.039	0.581	7786						$4D(\frac{7}{2}^+)$	1.521	0.639	8131
0 0 0 1 1					$1S(\frac{3}{2}^+)$	0.375	0.446	7079	3 0 3 0 3					$1F(\frac{5}{2}^-)$	0.877	0.510	7716
					$2S(\frac{3}{2}^+)$	0.677	0.542	7474						$2F(\frac{5}{2}^-)$	1.011	0.532	7979
					$3S(\frac{3}{2}^+)$	0.441	0.782	7568						$3F(\frac{5}{2}^-)$	0.933	0.871	8155
					$4S(\frac{3}{2}^+)$	1.048	0.596	7803						$4F(\frac{5}{2}^-)$	1.685	0.621	8236
1 0 1 0 1					$1P(\frac{1}{2}^-)$	0.557	0.465	7331	3 0 3 0 3					$1F(\frac{7}{2}^-)$	0.889	0.546	7754
					$2P(\frac{1}{2}^-)$	0.829	0.524	7649						$2F(\frac{7}{2}^-)$	1.021	0.567	8018
					$3P(\frac{1}{2}^-)$	0.607	0.818	7806						$3F(\frac{7}{2}^-)$	0.938	0.900	8183
					$4P(\frac{1}{2}^-)$	1.301	0.599	7958						$4F(\frac{7}{2}^-)$	1.678	0.652	8263
1 0 1 0 1					$1P(\frac{3}{2}^-)$	0.561	0.481	7353	4 0 4 1 3					$1G(\frac{5}{2}^+)$	1.019	0.532	7879
					$2P(\frac{3}{2}^-)$	0.832	0.539	7668						$2G(\frac{5}{2}^+)$	1.078	0.539	8141
					$3P(\frac{3}{2}^-)$	0.608	0.830	7819						$3G(\frac{5}{2}^+)$	1.069	0.896	8303
					$4P(\frac{3}{2}^-)$	1.308	0.613	7973						$4G(\frac{5}{2}^+)$	1.822	0.631	8364
2 0 2 1 1					$1D(\frac{1}{2}^+)$	0.718	0.494	7543	4 0 4 1 3					$1G(\frac{7}{2}^+)$	1.029	0.568	7914
					$2D(\frac{1}{2}^+)$	0.932	0.534	7822						$2G(\frac{7}{2}^+)$	1.095	0.575	8178
					$3D(\frac{1}{2}^+)$	0.771	0.849	7997						$3G(\frac{7}{2}^+)$	1.074	0.925	8330
					$4D(\frac{1}{2}^+)$	1.516	0.618	8109						$4G(\frac{7}{2}^+)$	1.808	0.661	8390
2 0 2 1 1					$1D(\frac{3}{2}^+)$	0.723	0.510	7562	4 0 4 1 4					$1G(\frac{7}{2}^+)$	1.020	0.526	7872
					$2D(\frac{3}{2}^+)$	0.935	0.548	7839						$2G(\frac{7}{2}^+)$	1.079	0.534	8135
					$3D(\frac{3}{2}^+)$	0.773	0.862	8010						$3G(\frac{7}{2}^+)$	1.070	0.892	8298
					$4D(\frac{3}{2}^+)$	1.518	0.632	8122						$4G(\frac{7}{2}^+)$	1.822	0.626	8359
2 0 2 1 2					$1D(\frac{3}{2}^+)$	0.720	0.489	7538	4 0 4 1 4					$1G(\frac{9}{2}^+)$	1.033	0.572	7917
					$2D(\frac{3}{2}^+)$	0.933	0.529	7818						$2G(\frac{9}{2}^+)$	1.102	0.580	8183
					$3D(\frac{3}{2}^+)$	0.775	0.846	7994						$3G(\frac{9}{2}^+)$	1.078	0.929	8332
					$4D(\frac{3}{2}^+)$	1.518	0.613	8105						$4G(\frac{9}{2}^+)$	1.803	0.665	8392
2 0 2 1 2					$1D(\frac{5}{2}^+)$	0.729	0.516	7569	4 0 4 1 5					$1G(\frac{9}{2}^+)$	1.023	0.521	7865
					$2D(\frac{5}{2}^+)$	0.937	0.553	7847						$2G(\frac{9}{2}^+)$	1.080	0.529	8130
					$3D(\frac{5}{2}^+)$	0.778	0.866	8015						$3G(\frac{9}{2}^+)$	1.073	0.889	8292
					$4D(\frac{5}{2}^+)$	1.519	0.636	8126						$4G(\frac{9}{2}^+)$	1.820	0.620	8353
2 0 2 1 3					$1D(\frac{5}{2}^+)$	0.726	0.485	7535	4 0 4 1 5					$1G(\frac{11}{2}^+)$	1.038	0.577	7920
					$2D(\frac{5}{2}^+)$	0.935	0.524	7816						$2G(\frac{11}{2}^+)$	1.111	0.586	8189
					$3D(\frac{5}{2}^+)$	0.783	0.844	7993						$3G(\frac{11}{2}^+)$	1.082	0.933	8333
					$4D(\frac{5}{2}^+)$	1.520	0.608	8101						$4G(\frac{11}{2}^+)$	1.795	0.667	8394

TABLE IV: The root mean square radii (fm) and mass spectra (MeV) of the Ω_{bc} family.

l_ρ	l_λ	L	s	j	$nL(J^P)$	$\langle r_\rho^2 \rangle^{1/2}$	$\langle r_\lambda^2 \rangle^{1/2}$	mass	l_ρ	l_λ	L	s	j	$nL(J^P)$	$\langle r_\rho^2 \rangle^{1/2}$	$\langle r_\lambda^2 \rangle^{1/2}$	mass
0 0 0 0 0					$1S(\frac{1}{2}^+)$	0.363	0.438	7055	3 0 3 1 2					$1F(\frac{3}{2}^-)$	0.874	0.515	7722
					$2S(\frac{1}{2}^+)$	0.666	0.538	7457						$2F(\frac{3}{2}^-)$	1.010	0.537	7984
					$3S(\frac{1}{2}^+)$	0.433	0.774	7550						$3F(\frac{3}{2}^-)$	0.929	0.875	8160
					$4S(\frac{1}{2}^+)$	1.026	0.591	7788						$4F(\frac{3}{2}^-)$	1.686	0.627	8241
1 0 1 1 0					$1P(\frac{1}{2}^-)$	0.549	0.474	7337	3 0 3 1 2					$1F(\frac{5}{2}^-)$	0.882	0.541	7749
					$2P(\frac{1}{2}^-)$	0.826	0.534	7655						$2F(\frac{5}{2}^-)$	1.016	0.562	8011
					$3P(\frac{1}{2}^-)$	0.597	0.824	7807						$3F(\frac{5}{2}^-)$	0.933	0.895	8180
					$4P(\frac{1}{2}^-)$	1.293	0.608	7964						$4F(\frac{5}{2}^-)$	1.681	0.648	8261
1 0 1 1 1					$1P(\frac{1}{2}^-)$	0.552	0.464	7327	3 0 3 1 3					$1F(\frac{5}{2}^-)$	0.876	0.510	7715
					$2P(\frac{1}{2}^-)$	0.827	0.524	7647						$2F(\frac{5}{2}^-)$	1.010	0.532	7978
					$3P(\frac{1}{2}^-)$	0.602	0.817	7803						$3F(\frac{5}{2}^-)$	0.932	0.871	8155
					$4P(\frac{1}{2}^-)$	1.296	0.599	7957						$4F(\frac{5}{2}^-)$	1.686	0.621	8236
1 0 1 1 1					$1P(\frac{3}{2}^-)$	0.557	0.480	7349	3 0 3 1 3					$1F(\frac{7}{2}^-)$	0.887	0.546	7754
					$2P(\frac{3}{2}^-)$	0.830	0.539	7665						$2F(\frac{7}{2}^-)$	1.020	0.567	8017
					$3P(\frac{3}{2}^-)$	0.603	0.829	7816						$3F(\frac{7}{2}^-)$	0.937	0.900	8183
					$4P(\frac{3}{2}^-)$	1.303	0.613	7971						$4F(\frac{7}{2}^-)$	1.678	0.652	8263
1 0 1 1 2					$1P(\frac{3}{2}^-)$	0.563	0.460	7330	3 0 3 1 4					$1F(\frac{7}{2}^-)$	0.880	0.505	7710
					$2P(\frac{3}{2}^-)$	0.832	0.519	7648						$2F(\frac{7}{2}^-)$	1.012	0.526	7974
					$3P(\frac{3}{2}^-)$	0.614	0.816	7807						$3F(\frac{7}{2}^-)$	0.936	0.868	8151
					$4P(\frac{3}{2}^-)$	1.309	0.595	7957						$4F(\frac{7}{2}^-)$	1.685	0.616	8231
1 0 1 1 2					$1P(\frac{5}{2}^-)$	0.571	0.488	7366	3 0 3 1 4					$1F(\frac{9}{2}^-)$	0.894	0.552	7759
					$2P(\frac{5}{2}^-)$	0.837	0.544	7679						$2F(\frac{9}{2}^-)$	1.025	0.572	8024
					$3P(\frac{5}{2}^-)$	0.616	0.835	7829						$3F(\frac{9}{2}^-)$	0.943	0.904	8186
					$4P(\frac{5}{2}^-)$	1.318	0.618	7981						$4F(\frac{9}{2}^-)$	1.675	0.655	8266
2 0 2 0 2					$1D(\frac{3}{2}^+)$	0.723	0.489	7539	4 0 4 0 4					$1G(\frac{7}{2}^+)$	1.021	0.526	7872
					$2D(\frac{3}{2}^+)$	0.934	0.529	7819						$2G(\frac{7}{2}^+)$	1.079	0.534	8135
					$3D(\frac{3}{2}^+)$	0.777	0.847	7995						$3G(\frac{7}{2}^+)$	1.071	0.892	8297
					$4D(\frac{3}{2}^+)$	1.519	0.613	8105						$4G(\frac{7}{2}^+)$	1.821	0.626	8358
2 0 2 0 2					$1D(\frac{5}{2}^+)$	0.731	0.516	7570	4 0 4 0 4					$1G(\frac{9}{2}^+)$	1.034	0.573	7917
					$2D(\frac{5}{2}^+)$	0.938	0.554	7848						$2G(\frac{9}{2}^+)$	1.103	0.581	8183
					$3D(\frac{5}{2}^+)$	0.781	0.867	8016						$3G(\frac{9}{2}^+)$	1.078	0.929	8331
					$4D(\frac{5}{2}^+)$	1.519	0.636	8126						$4G(\frac{9}{2}^+)$	1.802	0.664	8392

TABLE V: Fitted values of the slope (α) and intercept (β) of the Regge trajectories for the Ξ'_{bc} (Ξ_{bc}) and Ω'_{bc} (Ω_{bc}) families.

Trajectory	$\alpha(\text{GeV}^2)$	$\beta(\text{GeV}^2)$	$\alpha(\text{GeV}^2)$	$\beta(\text{GeV}^2)$
	Ξ'_{bc}			Ω'_{bc}
$n = 1(NP)$	3.099 ± 0.191	47.409 ± 0.548	3.193 ± 0.198	48.800 ± 0.568
$n = 2(NP)$	2.780 ± 0.059	52.778 ± 0.170	2.832 ± 0.065	54.354 ± 0.187
$n = 3(NP)$	3.005 ± 0.179	54.660 ± 0.515	3.054 ± 0.181	56.129 ± 0.520
$n = 1(UP)$	2.632 ± 0.097	51.014 ± 0.222	2.739 ± 0.102	52.540 ± 0.234
$n = 2(UP)$	2.483 ± 0.009	55.595 ± 0.020	2.556 ± 0.016	57.256 ± 0.037
$n = 3(UP)$	2.581 ± 0.097	58.237 ± 0.222	2.637 ± 0.098	59.776 ± 0.225
	Ξ_{bc}			Ω_{bc}
$n = 1(NP)$	3.097 ± 0.183	47.415 ± 0.526	3.193 ± 0.191	48.796 ± 0.550
$n = 2(NP)$	2.770 ± 0.048	52.812 ± 0.137	2.823 ± 0.055	54.379 ± 0.159
$n = 3(NP)$	3.021 ± 0.184	54.600 ± 0.527	3.068 ± 0.187	56.074 ± 0.537
$n = 1(UP)$	2.643 ± 0.107	50.984 ± 0.244	2.754 ± 0.113	52.496 ± 0.258
$n = 2(UP)$	2.495 ± 0.020	55.563 ± 0.046	2.562 ± 0.024	57.237 ± 0.054
$n = 3(UP)$	2.588 ± 0.110	58.210 ± 0.252	2.644 ± 0.111	59.749 ± 0.255

TABLE VI: The predicted masses (in MeV) of $1S$ states in this work and some other theoretical methods. The average values (\bar{m}) are calculated based on the mass values referenced here. The difference values in the brackets are calculated from \bar{m} .

State	$1S(\frac{1}{2}^+) (\Xi'_{bc})$	$1S(\frac{3}{2}^+) (\Xi'^{*}_{bc})$	$1S(\frac{1}{2}^+) (\Xi_{bc})$	$1S(\frac{1}{2}^+) (\Omega'_{bc})$	$1S(\frac{3}{2}^+) (\Omega'^{*}_{bc})$	$1S(\frac{1}{2}^+) (\Omega_{bc})$
[30]	6948(35)	6973(-1)	6922(-9)	7047(27)	7066(-8)	7011(-15)
[33]	6880(-33)	6980(6)	6970(39)	6960(-60)	7060(-14)	7050(24)
[35]	6934(21)	-	-	7033(13)	-	-
[37]	6805(-108)	6835(-139)	6787(-144)	6906(-114)	6930(-144)	6893(-133)
[38]	6953(40)	7044(70)	7015(84)	7064(44)	7142(68)	7116(90)
[39]	-	-	6930(-1)	-	-	7017(-9)
[41]	6890(-23)	6930(-44)	6930(-1)	7010(-10)	7040(-34)	7040(14)
[43]	6958(45)	6991(17)	-	7137(117)	7170(96)	-
[46]	6915(2)	7003(29)	-	-	-	-
[47]	6820(-93)	6900(-74)	6850(-81)	6930(-90)	7000(-74)	6970(-56)
[48]	6800(-113)	6850(-124)	6870(-61)	6980(-40)	7020(-54)	7050(24)
[50]	6950(37)	7020(46)	7000(69)	7050(30)	7110(36)	7090(64)
[55]	7014(101)	7064(90)	7037(106)	-	-	-
[59]	6988(75)	7083(109)	-	7103(83)	7200(126)	-
[60]	6914(1)	-	6933(2)	-	-	-
[63]	6920(7)	6986(12)	-	-	-	-
\bar{m}	6913	6974	6931	7020	7074	7026
Our	6952(39)	6980(6)	6955(24)	7053(33)	7079(5)	7055(29)